Elastic and inelastic scattering of electrons reflected from solids: Effects on energy spectra

Arne L. Tofterup
Fysisk Institut, Odense Universitet, DK-5230 Odense M, Denmark
(Received 18 December 1984)

The effects of elastic and inelastic scattering on energy spectra of electrons reflected from solids have been investigated theoretically. The aim was to evaluate the spectrum in the vicinity of the elastic peak. Following Tougaard and Sigmund's approach [Phys. Rev. B 25, 4452 (1982)], the elastic and inelastic scattering events are separated as independent when calculating the flux of reflected electrons. The influence of elastic scattering is considered here in detail within the P_1 approximation of the Boltzmann transport equation, and the inelastic scattering is described by the Landau formula. A general expression for the energy spectrum as well as expressions for discrete and continuous energy spectra are derived. Comparisons are made with the continuous part of measured spectra and a reasonable agreement is seen.

I. INTRODUCTION

The influence of elastic and inelastic scattering on the energy spectra of electrons emitted from solids has recently been investigated[1,2] with attention to Auger-electron spectroscopy (AES) and x-ray photoelectron spectroscopy (XPS), which, among other spectroscopies, are widely used for the investigation of solid surfaces. Electron-energy-loss spectroscopy (EELS) of solids is also widely used for surface analysis,[3,4] where one has a plane-collimated source of electrons incident on the solid surface and where one measures the energy spectrum of reflected electrons. Common for these spectroscopies is a continuous background signal due to electrons which, on their way out of the solid, have suffered inelastic scattering events.

In quantitative analysis[1,5–7] where peak areas are determined the direct energy spectrum $N(E)dE$ is needed. Thus, the background signal as a part of the spectrum must be interpreted with the aim of determining line intensities. Empirical methods exist[7–12] for deconvoluting the spectrum of backscattered electrons resulting from bombarding the surface with monoenergetic electrons.

There exist several Monte Carlo simulations of the backscattering (reflection) of electrons at high incident energies ($\gtrsim 10$ keV) (Ref. 13), but only a few at the lower energies[14,15] usually applied in EELS and AES. It is, however, not simple from the simulations to extract physical constants describing the electron transport in a solid.

A theoretical description of the energy spectrum is needed for (i) extracting physical constants describing the electron transport in a solid, and (ii) for evaluation with respect to determination of the absolute elemental composition as well as depth information.

In the present work the elastic and inelastic scattering of incident, monoenergetic electrons reflected from solids is investigated theoretically with the aim of evaluating energy spectra. The region of primary energy to be described by the present theory is typically 500—3000 eV. The investigations are based upon theories of particle transport in random media.[1,16–20] The transport of reflected electrons is treated here in a P_L approximation,[17,18] which gives a better description of the elastic scattering than the diffusion approximation applied recently in XPS theory.[1] A similar treatment on photoelectrons (in XPS) in the P_L approximation is in preparation.

II. GENERAL

The physical situation is sketched in Fig. 1, where an incoming electron with energy E_0 and direction $\mathbf{\Omega}_0$ penetrates the planar surface of a semi-infinite solid. The electron has a certain probability of being backscattered from the solid with a kinetic energy (E,dE) into a direction $(\mathbf{\Omega},d^2\Omega)$. While moving in the solid, the electron may undergo both inelastic and elastic scattering events, the latter due to angular deflection on atoms, whereas inelastic scattering is due to electron-electron interactions which cause only very small angular deflections in comparison to elastic scattering of electrons.[1] Therefore, as long as only small relative energy losses are considered, the elastic and inelastic scattering events may be decoupled.[1] Elastic scattering events cause backscattering, and inelastic events are responsible for the energy loss of a backscattered electron.

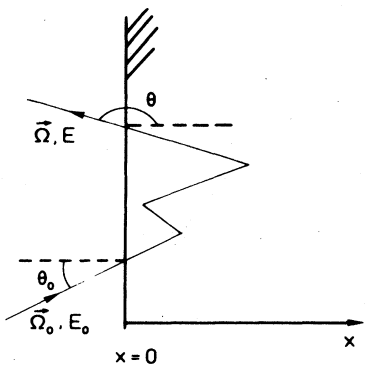

FIG. 1. Reflection of incident electron. Geometry and notation.

In order to account for angular deflections due to inelastic collisions, the elastic scattering cross section may be modified by changing Z^2 to $Z(Z+1)$ in the case of Coulomb scattering. However, at lower energies, which are going to be considered here, it is not so simple, and the cross section will therefore not be modified.

With a monodirectional and monoenergetic source of primary electrons hitting the surface ($x=0$) of the solid, one finds that the reflected electron flux $J(E,\Omega)dE\,d^2\Omega$ is given by[1]

$$J(E,\Omega)=\int dR\,Q(E_0,\Omega_0,x=0;R,\Omega)G(E_0,R;E)\,, \tag{1}$$

when elastic and inelastic scattering events are separated. Here,

$$Q(E_0,\Omega_0,x;R,\Omega)dR\,d^2\Omega$$

is the probability for an electron with primary energy E_0 and initial direction Ω_0 to pass a plane at depth x in direction $(\Omega,d^2\Omega)$ after having traveled a path length (R,dR) in the solid; $G(E_0,R;E)dE$ is the probability that the electron has energy (E,dE) after having traveled the path length R. Equation (1) assumes the total energy loss E_0-E to be small enough to allow one to ignore the dependence of elastic scattering cross sections on electron energy.[1] This assumption is justified to the extent that only the energy spectrum near the initial energy is analyzed.[3,4]

III. ELASTIC SCATTERING

This section serves to provide a reasonable estimate of the path-length distribution $Q(E_0,\Omega_0,x=0;R,\Omega)$ in Eq. (1). For that purpose the electron transport is first considered in an infinite medium, and afterwards is confined to a semi-infinite medium.

The motion of an electron in a homogeneous, random medium is characterized by a distribution function $F(\mathbf{r},\mathbf{v},t)d^3r\,d^3v$ in position $\mathbf{r}$ and velocity $\mathbf{v}$ at time t. The electron is assumed to have the initial velocity $\mathbf{v}_0$ at time $t=0$ when it is at $\mathbf{r}=\mathbf{0}$, i.e.,

$$F(\mathbf{r},\mathbf{v},0)=\delta(\mathbf{r})\delta(\mathbf{v}-\mathbf{v}_0)\,, \tag{2}$$

where δ is the Dirac function.

The function F obeys Boltzmann's transport equation, which is used here in the forward form,

$$\left[-\frac{\partial}{\partial t}-\mathbf{v}\cdot\nabla\right]F(\mathbf{r},\mathbf{v},t) =N\int d^3v'[vF(\mathbf{r},\mathbf{v},t)K(\mathbf{v},\mathbf{v}')-v'F(\mathbf{r},\mathbf{v}',t)K(\mathbf{v}',\mathbf{v})] \tag{3}$$

where $\mathbf{v}'$ is the velocity after a scattering event with differential cross section $d\sigma=K(\mathbf{v},\mathbf{v}')d^3v'$. N is the density of scattering centers.

We assume planar geometry, ignore energy loss, and integrate over the azimuthal variable, which is justified when the experimental data are from, e.g., a cylindrical mirror energy analyzer (CMA); then (2) and (3) yield[1]

$$\left[-\frac{\partial}{\partial R}-\eta\frac{\partial}{\partial x}\right]F(x,\eta,R) =N\int d\sigma[F(x,\eta,R)-F(x,\eta',R)] \tag{4}$$

and

$$F(x,\eta,0)=\delta(x)\delta(\eta-\eta_0)\,, \tag{5}$$

where $R=vt$ is the path length, $\eta_0=\cos\theta_0$ and $\eta=\cos\theta$ (Fig. 1) are direction cosines with respect to the x axis, and $d\sigma$ is now the differential cross section for angular deflection only. To separate the angular dependence it is common to expand F in terms of Legendre polynomials, i.e.,

$$F(x,\eta,R)=\sum_l(2l+1)F_l(x,R)P_l(\eta)\,. \tag{6}$$

Equation (6) inserted into (4) and (5) yields[20]

$$-(2l+1)\frac{\partial}{\partial R}F_l-(l+1)\frac{\partial}{\partial x}F_{l+1}-l\frac{\partial}{\partial x}F_{l-1} =(2l+1)N\sigma_lF_l(x,R) \tag{7}$$

and

$$F_l(x,0)=\tfrac{1}{2}\delta(x)P_l(\eta_0)\,, \tag{8}$$

where

$$\sigma_l=\int d\sigma[1-P_l(\cos\phi)] \tag{9}$$

is the transport cross section of order l, and ϕ is the scattering angle in the laboratory system.

Equation (7) represents an infinite set of coupled, partial differential equations. In the following, a diffusion solution to Eq. (4) or (7) is considered briefly, and the P_L approximation[17,18] which reduces (7) to a manageable set of equations is considered in detail.

A. Diffusion solution

For a homogeneous, infinite medium the nth moment of the distribution function, defined by

$$F_l^n(R)=\int_{-\infty}^{\infty}dx\,x^nF_l(x,R)\,, \tag{10}$$

may be calculated following Ref. 1. The results for the first three moments are

$$F^0(R)=1\,, \tag{11}$$

$$\langle x\rangle=\eta_0\lambda_1(1-e^{-R/\lambda_1})\,, \tag{12}$$

and

$$\langle(\Delta x)^2\rangle=\langle x^2\rangle-\langle x\rangle^2=\tfrac{2}{3}\lambda_1^2\left[\frac{R}{\lambda_1}-(1-e^{-R/\lambda_1})-\tfrac{3}{2}\eta_0^2(1-e^{-R/\lambda_1})^2 +\frac{(3\eta_0^2-1)\lambda_2}{(\lambda_1-\lambda_2)\lambda_1}[\lambda_1(1-e^{-R/\lambda_1})-\lambda_2(1-e^{-R/\lambda_2})]\right], \tag{13}$$

TABLE I. Values of transport mean free paths λ_1 and λ_2, calculated from Ref. 28.

		E (eV)			
		500[a]	1000	2000	4000
Al	λ_1 (Å)	52	140	413	1290
	λ_2 (Å)	37	84	210	590
Si	λ_1 (Å)	57	154	443	1370
	λ_2 (Å)	41	93	228	633
Ni	λ_1 (Å)	17	35	92	256
	λ_2 (Å)	15	29	59	140
Pt	λ_1 (Å)	15	23	43	98
	λ_2 (Å)	16	25	47	83

[a]Extrapolated from data of Ref. 28.

where

$$\lambda_l=(N\sigma_l)^{-1}\,. \tag{14}$$

Values for λ_1 and λ_2 based upon atomic scattering cross sections are listed in Table I for silicon and some typical metals at several electron energies. For large path lengths $R\gg\lambda_1,\lambda_2$, one gets the diffusionlike asymptotic behavior from (12) and (13),

$$\langle x\rangle\simeq\eta_0\lambda_1\,, \tag{15}$$

$$\langle(\Delta x)^2\rangle\simeq 2D(t-t_0)\,, \tag{16}$$

with the diffusion coefficient

$$D=\tfrac{1}{3}v\lambda_1 \tag{17}$$

and delay time

$$t_0=\frac{\lambda_1}{v}[1+\tfrac{3}{2}\eta_0^2-(3\eta_0^2-1)\lambda_2/\lambda_1]\,, \tag{18}$$

depending on η_0 and the ratio λ_2/λ_1.

The variance, Eq. (13), and the asymptotic expression, Eq. (16), are plotted in Fig. 2 for normal incidence ($\eta_0=1$) and several values of λ_2/λ_1. It is seen that t_0 is zero for $\lambda_2/\lambda_1=\frac{5}{4}$ and $\eta_0=1$, and the variance is given by $2Dt$ to a good approximation, but the depth distribution in an infinite medium approaches a diffusion profile only if Eqs. (15) and (16) are valid,

$$F(x,t)=\frac{1}{[2\pi\langle(\Delta x)^2\rangle]^{1/2}}\exp\left[-\frac{(x-\langle x\rangle)^2}{2\langle(\Delta x)^2\rangle}\right]\,, \tag{19}$$

which is the case when $R\gtrsim 2\lambda_1$, cf. Fig. 2 and Ref. 1.

Within the validity of Eq. (19), one may write the path-length distribution

$$Q_d(E_0,\eta_0,x=0;R,\eta)dR\,d\eta$$

for an electron in a semi-infinite medium,[1] assuming the Knudsen cosine law for the angular distribution,

$$Q_d(E_0,\eta_0,x=0;R,\eta)=2\eta\left[\frac{3\eta_0^2\lambda_1}{4\pi(R-R_0)^3}\right]^{1/2}\exp\left[-\frac{3\eta_0^2\lambda_1}{4(R-R_0)}\right]\,, \tag{20}$$

where $R_0=vt_0$. Equation (20) is plotted in Fig. 3 for several values of R_0, cf. Fig. 2. The presence of $\eta_0\lambda_1$ in

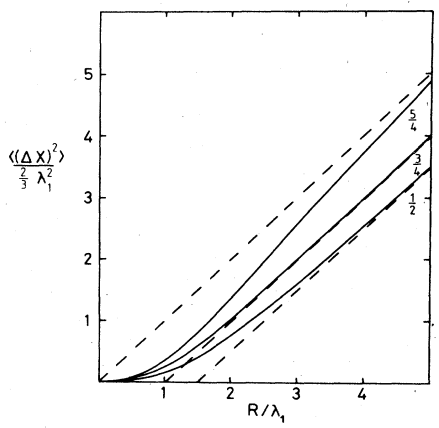

FIG. 2. Variance of elastic scattering depth distribution shown for normal incidence and λ_2/λ_1 equal to $\frac{5}{4}$, $\frac{3}{4}$, and $\frac{1}{2}$, respectively. Solid curves: $\langle(\Delta x)^2\rangle$ according to Eq. (13). The asymptotic behavior, Eq. (16), is indicated by the dashed curves.

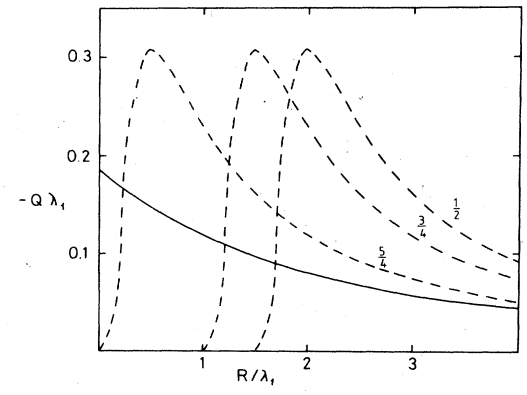

FIG. 3. Calculated angular integrated path-length distributions in semi-infinite medium for normal incidence. Dashed curves: distribution in the diffusion approximation, Eq. (20), with λ_2/λ_1 as in Fig. 2. Solid curve: distribution in P_1 approximation, Eq. (41).

(20) is due to the anisotropic source, whereas R_0 appears because Eq. (20) is a better approximation than that in Ref. 1.

B. P_1 approximation

As the diffusion solution is not valid at small path lengths, a better approximation to the distribution function must be inferred; the P_L approximation demands that[17,18,21]

$$F_l \equiv 0, \quad l > L \tag{21}$$

in the set of equations, Eq. (7). Equations (7) and (21) then constitute the so-called P_L equations. Thus, the P_1 equations solved here are

$$\begin{aligned} &\frac{\partial}{\partial R}F_0(x,R)+\frac{\partial}{\partial x}F_1(x,R)=0\ , \\ &-3\frac{\partial}{\partial R}F_1(x,R)-\frac{\partial}{\partial x}F_0(x,R)=3N\sigma_1 F_1(x,R)\ , \end{aligned} \tag{22}$$

with the initial condition (8).

The Laplace transform $F_l(x,s)$ of (22) with respect to R satisfies

$$\begin{aligned} &sF_0(x,s)-\tfrac{1}{2}\delta(x)+\frac{\partial}{\partial x}F_1(x,s)=0\ , \\ &-3sF_1(x,s)+\tfrac{3}{2}\eta_0\delta(x)-\frac{\partial}{\partial x}F_0(x,s)=3N\sigma_1 F_1(x,s)\ . \end{aligned} \tag{23}$$

1. *Solution for infinite medium*

For the infinite medium, Fourier transformation with respect to x of (23) gives a set of algebraic equations with the solutions

$$F_0(k,s)=\frac{\frac{3}{2}(s+N\sigma_1)-\frac{3}{2}\eta_0 ik}{k^2+3s(s+N\sigma_1)} \tag{24}$$

and

$$F_1(k,s)=\frac{\frac{3}{2}\eta_0 s-\frac{1}{2}ik}{k^2+3s(s+N\sigma_1)}\ . \tag{25}$$

Fourier inversion then yields

$$F_0(x,s)=\left[\pm\frac{3}{4}\eta_0+\frac{\sqrt{3}}{4}\left[\frac{s+N\sigma_1}{s}\right]^{1/2}\right]\times\exp\{\mp[3s(s+N\sigma_1)]^{1/2}x\} \tag{26}$$

and

$$F_1(x,s)=\left[\pm\frac{1}{4}+\frac{\sqrt{3}}{4}\eta_0\left[\frac{s}{s+N\sigma_1}\right]^{1/2}\right]\times\exp\{\mp[3s(s+N\sigma_1)]^{1/2}x\} \tag{27}$$

for $x \gtrless 0$, respectively.

If one is interested mainly in the distribution function at $x=0$, it is sufficient to Laplace-invert (26) and (27) for $x=0^+$ (cf. Fig. 1); i.e.,

$$F_0(0^+,R)=\left[\frac{\sqrt{3}}{4}+\frac{3}{4}\eta_0\right]\delta(R)+\frac{\sqrt{3}}{8}\lambda_1^{-1}e^{-R/2\lambda_1}\times[I_0(\tfrac{1}{2}R/\lambda_1)+I_1(\tfrac{1}{2}R/\lambda_1)] \tag{28}$$

and

$$F_1(0^+,R)=\tfrac{1}{4}\delta(R)-\frac{\sqrt{3}}{8}\eta_0\lambda_1^{-1}e^{-R/2\lambda_1}\times[I_0(\tfrac{1}{2}R/\lambda_1)-I_1(\tfrac{1}{2}R/\lambda_1)]\ , \tag{29}$$

where I_0 and I_1 are modified Bessel functions of the first kind. According to Eq. (6), the distribution function at $x=0$ in the P_1 approximation is then given by

$$F(0^+,\eta,R)=F_0(0^+,R)+3\eta F_1(0^+,R)\ . \tag{30}$$

Thus, the angle-integrated distribution function is

$$\begin{aligned} \int_{-1}^{1}d\eta\,F(0^+,\eta,R)&=2F_0(0^+,R) \\ &=\frac{\sqrt{3}}{4}\lambda_1^{-1}e^{-R/2\lambda_1}[I_0(\tfrac{1}{2}R/\lambda_1)+I_1(\tfrac{1}{2}R/\lambda_1)]\ , \end{aligned} \tag{31}$$

where the δ function in (28) is neglected, as we are only interested in particles with a finite path length. Inserting the asymptotic expressions for I_0 and I_1 (Ref. 22) into Eq. (31), we find, in the limit $R \gg \lambda_1$,

$$\left[\frac{3}{4\pi\lambda_1 R}\right]^{1/2}, \tag{32}$$

which is identical to the leading term in the diffusion solution, Eq. (19), with (15) and (16) inserted.

Consider Eq. (22), neglecting the term $(\partial/\partial R)F_1(x,R)$ in comparison to $N\sigma_1 F_1(x,R)$,[18] and solve for F_0 and F_1. One then finds that $F_0(x,R)$ and $F_1(x,R)$ are the depth distribution for a source at $x=0$ and the particle flux for the same source, respectively, in the diffusion approximation. The difference between the P_1 solution and the diffusion solution for the infinite medium may thus be visualized by comparing $(\partial/\partial R)F_1(0^+,R)$ with $\lambda_1^{-1}F_1(0^+,R)$, determined by Eq. (29). The expression

$$\begin{aligned} f(R)&=\frac{(\partial/\partial R)F_1(0^+,R)}{\lambda_1^{-1}F_1(0^+,R)} \\ &=-1+\frac{I_1(\frac{1}{2}R/\lambda_1)}{(R/\lambda_1)[I_0(\frac{1}{2}R/\lambda_1)-I_1(\frac{1}{2}R/\lambda_1)]} \end{aligned} \tag{33}$$

is plotted versus R/λ_1 in Fig. 4, which shows that only after relatively large path lengths is it reasonable to

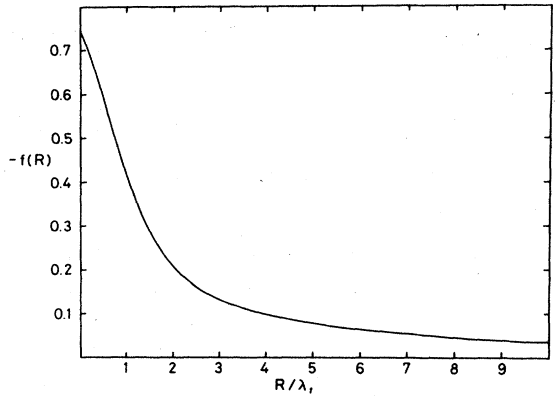

FIG. 4. The significance of $(\partial/\partial R)F_1$ expressed by $f(R)$, Eq. (33).

neglect the time variation $(\partial/\partial R)F_1(x,R)$ of the current term F_1.

2. *Solution for semi-infinite medium*

Consider the homogeneous set of equations corresponding to (23). For $x>0$ the solution is

$$F_0^{\text{hom}}(x,s)=a(s)\sqrt{3}\left[\frac{s+N\sigma_1}{s}\right]^{1/2}\times\exp\{-[3s(s+N\sigma_1)]^{1/2}x\} \tag{34}$$

and

$$F_1^{\text{hom}}(x,s)=a(s)\exp\{-[3s(s+N\sigma_1)]^{1/2}x\}\ , \tag{35}$$

where $a(s)$ is independent of x. The solution for the semi-infinite medium, at $x=0$, can in general be written as

$$F(0,\eta,R)=F^{\text{inhom}}(0,\eta,R)+F^{\text{hom}}(0,\eta,R)\ , \tag{36}$$

where F^{inhom} can, e.g., be given by (30).

To determine $a(s)$, a boundary condition must be inferred, cf. Ref. 23 or Appendix A, viz.,

$$F(0,\eta,R)=\frac{1}{\eta_0}\delta(R)\delta(\eta-\eta_0),\quad \eta>0 \tag{37}$$

which may be considered as a condition for the particle flux into the medium. Because the distribution function is expanded here only into a finite set of Legendre polynomials, it is reasonable to reduce Eq. (37) to a Marshak condition[17,18,21] for the net flux into the medium, as will be seen below, Eq. (48); i.e., for the Laplace transform,

$$\int_0^1 d\eta\,\eta F(0,\eta,s)=\tfrac{1}{2}F_0(0,s)+F_1(0,s)=\frac{1}{2}+\frac{1}{4\eta_0} \tag{38}$$

in the P_1 approximation, as $F_l(0,s)=(1/2\eta_0)P_l(\eta_0)$ according to (37). Insertion of Eqs. (26), (27), (34), and (35) into (38) yields

$$a(s)=-\frac{1}{4}-\frac{\sqrt{3}}{4}\eta_0\left[\frac{s}{s+N\sigma_1}\right]^{1/2}+\frac{\frac{1}{2}+1/4\eta_0}{1+\sqrt{3}/2[(s+N\sigma_1)/s]^{1/2}} \tag{39}$$

for $a(s)$.

Finally, from Eq. (36),

$$F(0,\eta,s)=1+\frac{1}{2\eta_0}-\frac{(1+1/2\eta_0)(1-\frac{3}{2}\eta)}{1+\sqrt{3}/2[(s+N\sigma_1)/s]^{1/2}}\ . \tag{40}$$

Laplace inversion of (40), cf. Appendix B, yields

$$Q(F_0,\eta_0,x=0;R,\eta)=\frac{2\sqrt{3}}{\pi}\left[1+\frac{1}{2\eta_0}\right](\eta-\tfrac{3}{2}\eta^2)\lambda_1^{-1}\times\int_0^1 du\,e^{-uR/\lambda_1}\frac{\sqrt{u(1-u)}}{u+3} \tag{41}$$

for the path-length distribution, where $u=-s\lambda_1$ and terms with $\delta(R)$ have been neglected.

a. Total flux. For the total flux of elastically backscattered electrons, Eq. (41) yields

$$\int_{-1}^0 d\eta\int_0^\infty dR\,Q(E_0,\eta_0,x=0;R,\eta)=-2(2-\sqrt{3})\left[1+\frac{1}{2\eta_0}\right], \tag{42}$$

which is $\simeq -0.8038$ for $\eta_0=1$. The flux is negative because it goes in the negative x direction. Equation (42) predicts a reflected flux beyond 1 for $\theta_0>55°$. Therefore, the expression for the path-length distribution should only be applied at near-normal incidence.

b. Differential flux. We present the following.

(i) Numerical calculation. The integrand in Eq. (41) is suitable for a Gaussian integration[22] as

$$\int_0^1 du\,e^{-uR/\lambda_1}\frac{\sqrt{u(1-u)}}{u+3}\simeq\tfrac{1}{4}\sum_{i=1}^n w_i\frac{e^{-u_iR/\lambda_1}}{u_i+3}\ , \tag{43}$$

where

$$u_i=\tfrac{1}{2}+\tfrac{1}{2}\cos\left[\frac{i\pi}{n+1}\right],$$

and

$$w_i=\frac{\pi}{n+1}\sin^2\left[\frac{i\pi}{n+1}\right].$$

Figure 3 shows the path-length distribution, Eq. (41), together with the diffusion solution, Eq. (20), with $\eta_0=1$ integrated over η from -1 to 0.

With reasonable accuracy the summation in Eq. (43) may, for simplicity, be approximated by a single exponential in the region $0\le R\lesssim 3\lambda_1$. One finds the approximate expression

$$Q(E_0,\eta_0,x=0;R,\eta)$$
$$=\frac{\sqrt{3}}{(2+\sqrt{3})^2}\left[1+\frac{1}{2\eta_0}\right](\eta-\tfrac{3}{2}\eta^2)\lambda_1^{-1}\exp(-\alpha R/\lambda_1) \tag{44}$$

for the path-length distribution, Eq. (41). Equation (44) is plotted in Fig. 5 with $\alpha=0.42$.

(ii) Analytical calculation for small path lengths. For small path lengths corresponding to $s \gg N\sigma_1$, Eq. (40) is approximated according to

$$\frac{1}{1+\sqrt{3}/2[(s+N\sigma_1)/s]^{1/2}}$$
$$\simeq\frac{1}{1+\sqrt{3}/2}-\frac{\sqrt{3}N\sigma_1}{(2+\sqrt{3})^2}\left[\frac{1}{s}-(\sqrt{3}-\tfrac{5}{4})\frac{N\sigma_1}{s^2}+\cdots\right],$$

and it is found that

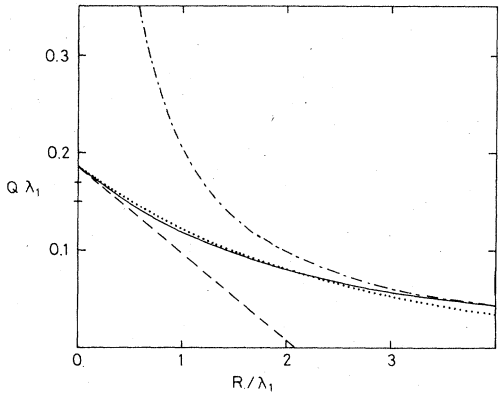

FIG. 5. Calculated angular integrated P_1-path-length distribution for normal incidence. Solid curve: numerical calculation according to Eqs. (41) and (43). Dotted curve: the exponential, Eq. (44), as an approximation to the path-length distribution. Dashed line: analytical expression for small path lengths, Eq. (45). Dashed-dotted curve: analytical expressions for large path lengths, Eq. (46). The distribution for a single elastic collision is marked at $R=0$ for platinum and nickel, $E_0=1000$ eV. (The lowest value is for nickel.)

$$Q(E_0,\eta_0,x=0;R \text{ small},\eta)\simeq\frac{\sqrt{3}(1+1/2\eta_0)(\eta-\frac{3}{2}\eta^2)\lambda_1^{-1}}{(2+\sqrt{3})^2}[1-(\sqrt{3}-\tfrac{5}{4})R/\lambda_1+O((R/\lambda_1)^2)], \tag{45}$$

when terms with $\delta(R)$ are subtracted.

(iii) Analytical calculation for large path lengths. For $s \ll N\sigma_1$, (40) is approximated according to

$$\frac{1}{1+\sqrt{3}/2[(s+N\sigma_1)/s]^{1/2}}\simeq\frac{\sqrt{s}}{\sqrt{s}+\frac{1}{2}(3N\sigma_1)^{1/2}},$$

and one gets

$$Q(E_0,\eta_0,x=0;R \text{ large},\eta)\simeq\frac{1}{2}\left[\frac{3}{\pi}\right]^{1/2}\left[1+\frac{1}{2\eta_0}\right](\eta-\tfrac{3}{2}\eta^2)\lambda_1^{-1}\left[\frac{1}{(R/\lambda_1)^{1/2}}-\tfrac{1}{2}\sqrt{3\pi}e^{3R/4\lambda_1}\operatorname{erfc}(\tfrac{3}{4}R/\lambda_1)^{1/2}\right], \tag{46}$$

where

$$\operatorname{erfc}(z)=\frac{2}{\sqrt{\pi}}\int_z^\infty dt\, e^{-t^2} \tag{47}$$

is the complementary error function. Application of the asymptotic expansion of erfc(z) (Ref. 22) yields the leading term

$$Q(E_0,\eta_0,x=0;R \text{ large},\eta)$$
$$\sim\frac{1+1/2\eta_0}{\sqrt{3\pi}}(\eta-\tfrac{3}{2}\eta^2)\lambda_1^{-1}(R/\lambda_1)^{-3/2}, \tag{48}$$

which gives $(3\lambda_1/4\pi R^3)^{1/2}$ for $\eta_0=1$, integrated over η, i.e., the diffusion solution for $R \gg \lambda_1$, compare Eq. (20). This lends support to the use of the approximate boundary condition, Eq. (38). Expressions (45) and (48) integrated over η are plotted in Fig. 5 together with the path-length distribution, Eq. (41).

c. Angular distribution. In the P_1 approximation, the angular distribution

$$f_1(\theta)=(\cos\theta-\tfrac{3}{2}\cos^2\theta)\sin\theta \tag{49}$$

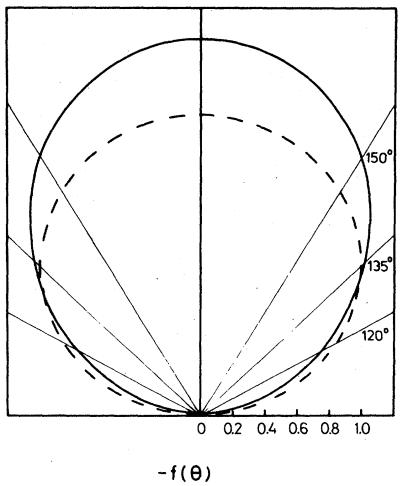

FIG. 6. Angular distribution. Solid curve: P_1 approximation, Eq. (49). Dashed curve: Knudsen's cosine law, Eq. (50).

was found, whereas Knudsen's cosine law reads

$$f_d(\theta)=2\cos\theta\sin\theta\ . \tag{50}$$

These two distributions are plotted in Fig. 6. It is seen that in the P_1 approximation the angular distribution is narrower in the direction normal to the surface.

IV. ENERGY DISTRIBUTION OF REFLECTED ELECTRONS

The electrons undergo multiple inelastic scattering when moving in the medium. An individual inelastic scattering event is characterized by an inverse differential mean free path $\kappa(E,T)$, where E is the kinetic energy of the electron and T is the energy loss. $\kappa(E,T)$ depends only weakly on E, at most as E^{-1} for free Coulomb scattering, so when measuring small relative energy losses the E dependence may be ignored.[1] In the following, κ is therefore considered as a function of T only. Then the energy-loss distribution for an electron with initial energy E_0 and path length R is given by Landau's formula[24]

$$G(E_0,R;E)=\frac{1}{2\pi}\int_{-\infty}^{\infty}dp\,\exp[ip\epsilon-R\sigma(p)]\ , \tag{51}$$

where

$$\epsilon=E_0-E \tag{52}$$

and

$$\sigma(p)=\int_0^{\infty}dT\,\kappa(T)(1-e^{-ipT})\ . \tag{53}$$

The energy distribution of reflected electrons is given by Eq. (1) which, after insertion of (41) and (51), yields the general result

$$J(E,\eta)=\frac{2\sqrt{3}}{\pi}\left[1+\frac{1}{2\eta_0}\right](\eta-\tfrac{3}{2}\eta^2)\times\frac{1}{2\pi}\int_{-\infty}^{\infty}dp\,e^{ip\epsilon}\int_0^1 du\frac{\sqrt{u(1-u)}}{(u+3)[u+\lambda_1\sigma(p)]}\ . \tag{54}$$

Values for the inelastic mean free path λ and stopping power S, defined by

$$\frac{1}{\lambda}=\int dT\,\kappa(T),\quad S=\int dT\,T\kappa(T)\ , \tag{55}$$

are calculated in, e.g., Refs. 25–27 and are shown in Table II for aluminum, silicon, nickel, and platinum at several electron energies. From these values and Table I, it may be concluded that, in as far as the energy loss of an electron is small compared to its initial energy, the mean path length ϵ/S will not exceed $\sim 2\lambda_1$. It would therefore not be reasonable to use the diffusion approximation. In that case the approximate expression for the path-length distribution [Eq. (44)] applies, and the energy distribution [Eq. (54)] may be replaced by the simpler expression

$$J(E,\eta)=\frac{\sqrt{3}}{(2+\sqrt{3})^2}\left[1+\frac{1}{2\eta_0}\right](\eta-\tfrac{3}{2}\eta^2)\times\frac{1}{2\pi}\int_{-\infty}^{\infty}dp\,e^{ip\epsilon}\frac{1}{\alpha+\lambda_1\sigma(p)}\ , \tag{56}$$

with $\alpha\simeq 0.42$.

A. Discrete energy-loss spectrum

For that part of the spectrum for which the path length R in Eq. (51) is small, $R\ll\lambda$, the integrand in (56) may be expanded in powers of κ according to

$$\frac{1}{\alpha+\lambda_1\sigma(p)}=\frac{1}{\alpha+\lambda_1/\lambda}\left[1+\frac{\lambda_1}{\alpha+\lambda_1/\lambda}\int dT\,\kappa(T)e^{-ipT}+\left[\frac{\lambda_1}{\alpha+\lambda_1/\lambda}\right]^2\int dT\,\kappa(T)\int dT'\,\kappa(T')e^{-ip(T+T')}+\cdots\right]. \tag{57}$$

By (56) and (57), the spectrum then becomes

$$J(E,\eta)=\frac{\sqrt{3}}{(2+\sqrt{3})^2}\left[1+\frac{1}{2\eta_0}\right](\eta-\tfrac{3}{2}\eta^2)\frac{1}{\alpha+\lambda_1/\lambda}\times\left[\delta(\epsilon)+\frac{\lambda_1\kappa(\epsilon)}{\alpha+\lambda_1/\lambda}+\left[\frac{\lambda_1}{\alpha+\lambda_1/\lambda}\right]^2\int dT\,\kappa(T)\kappa(\epsilon-T)+\cdots\right]. \tag{58}$$

In the considered energy region (500–3000 eV), for light elements such as, e.g., aluminum,[25–28] we have $\lambda_1\gg\lambda$. Hence, the constant α may be neglected in comparison to λ_1/λ, and (58) reduces to

$$J(E,\eta)\simeq\frac{\sqrt{3}}{(2+\sqrt{3})^2}\left[1+\frac{1}{2\eta_0}\right](\eta-\tfrac{3}{2}\eta^2)\frac{\lambda}{\lambda_1}\left[\delta(\epsilon)+\lambda\kappa(\epsilon)+\lambda^2\int dT\,\kappa(T)\kappa(\epsilon-T)+\cdots\right]. \tag{59}$$

This corresponds to neglecting the R dependence in the path-length distribution, Eq. (41), from the beginning. Equation (59) is then based upon a single elastic collision and is therefore an approximation to the single-collision distribution.

B. Continuum energy-loss spectrum

For larger energy losses where a continuum description of the energy loss is appropriate,[29] (53) may be expanded in powers of p. To second order one finds[1]

TABLE II. Values of inelastic mean free path and stopping power, from Ref. 25.

		E (ev)			
		500	1000	2000	3000
Al	λ (Å)	12	21	36	45
	S (eV/Å)	3.2	2.3	1.5	1.2
Si	λ (Å)	12	21	38	53
	S (eV/Å)	3.0	2.1	1.3	1.1
Ni	λ (Å)	8.0	14	25	33
	S (eV/Å)	7.0	5.3	3.9	3.0
Pt	λ (Å)	8.0	15	26	33
	S (eV/Å)	7.0	6.2	4.3	3.5

$$\sigma(p)\simeq ipS+\tfrac{1}{2}p^2W\,, \tag{60}$$

with S given by (55) and W, the straggling parameter,[29] defined by

$$W=\int dT\,T^2\kappa(T)\,. \tag{61}$$

The expansion (60) inserted into Eq. (51) yields a Gaussian energy-loss distribution[1] and, according to Ref. 29, this is reasonable at large path lengths. Insertion of Eq. (60) into (56) yields then the continuous spectrum

$$J(E,\eta)=\frac{\sqrt{3}}{(2+\sqrt{3})^2}\left[1+\frac{1}{2\eta_0}\right](\eta-\tfrac{3}{2}\eta^2)\times\frac{\exp\left\{-\dfrac{\epsilon S}{W}\left[\left[1+\dfrac{2\alpha W}{\lambda_1 S^2}\right]^{1/2}-1\right]\right\}}{\lambda_1 S\left[1+\dfrac{2\alpha W}{\lambda_1 S^2}\right]^{1/2}}\,. \tag{62}$$

For comparison, the path-length distribution in the diffusion approximation, Eq. (20), may be applied. Insert Eq. (60) into (51) (Ref. 1) and then insert Eqs. (20) and (51) into Eq. (1); with $R_0=0$ in Eq. (20) the spectrum then becomes

$$J_d(E,\eta)=2\eta\left[\frac{3\eta_0^2\lambda_1}{2\pi^2W}\right]^{1/2}\times\frac{Se^{\epsilon S/W}K_1[(S/W)(\epsilon^2+\frac{3}{2}\eta_0^2\lambda_1W)^{1/2}]}{(\epsilon^2+\frac{3}{2}\eta_0^2\lambda_1W)^{1/2}}\,, \tag{63}$$

where K_1 is a modified Bessel function of the second kind.

1. Evaluation of the straggling parameter

The nonrelativistic Møller cross section for the scattering of two free electrons is given by[30]

$$d\sigma(T)=\frac{\pi e^4dT}{E}\left[\frac{1}{T^2}+\frac{1}{(E-T)^2}-\frac{1}{T(E-T)}\right]. \tag{64}$$

In Eq. (61) the large energy losses dominate in the integral, and $\kappa(T)$ may then be identified with $NZ\,d\sigma(T)$. The upper integration limit is $\frac{1}{2}E$ in (61) because the primary electron to be detected is that with the largest energy. Thus, Eq. (61) reads

$$W=(\tfrac{5}{2}-3\ln 2)\pi e^4NZ\simeq(274\ \text{eV}^2\,\text{Å}^2)NZ\,. \tag{65}$$

2. Comparison with diffusion solution

The energy distributions, Eqs. (62) and (63), are plotted in Fig. 7 for several values of λ_1S and λ_1W, which, according to Tables I and II and Eq. (65), are representative for most solids in the region of primary energy (500—3000 eV) to be described by the present theory. In the plotted energy-loss region the two energy distributions deviate strongly in shape; the diffusional solution (63) has a pronounced maximum which may be due to the strong maximum in the path-length distribution, cf. Fig. 3. Furthermore, except for the lowest energy, where a continuum description is invalid, the energy distribution, Eq. (62), based upon the P_1 approximation, always yields a lower flux of reflected electrons. Only path lengths $R\lesssim\lambda_1$ are represented in Fig. 7, and therefore the diffusion description should not be applicable.

3. Comparison with measurements

The continuous spectrum, Eq. (62), and experimental points of the apparent EELS spectra,[31] are plotted in Fig. 8 for nickel and platinum, normalized at an energy loss of 125 and 150 eV for primary energies of 500 and 2000 eV, respectively. For the theoretical spectra, use has been made of parameter values according to Eq. (65) and Tables I and II.

The experimental points follow to some extent a straight line, although not exactly the plotted theoretical lines. However, in the plotted energy-loss region a reasonable agreement is seen, indicating that the intensity of reflected electrons falls off exponentially with energy loss according to Eq. (62), when the energy loss is small compared to the primary energy of the electron. The measured yields are usually not known with sufficient accuracy[14] to permit a comparison of absolute yields, and sometimes absolute yields are not measured at all. Therefore the above comparison was made only in arbitrary units.

V. DISCUSSION

It has already been mentioned that even for the optimal value of $\lambda_2/\lambda_1=\frac{5}{4}$, the diffusion solution breaks down when the mean path length of the considered electron is of

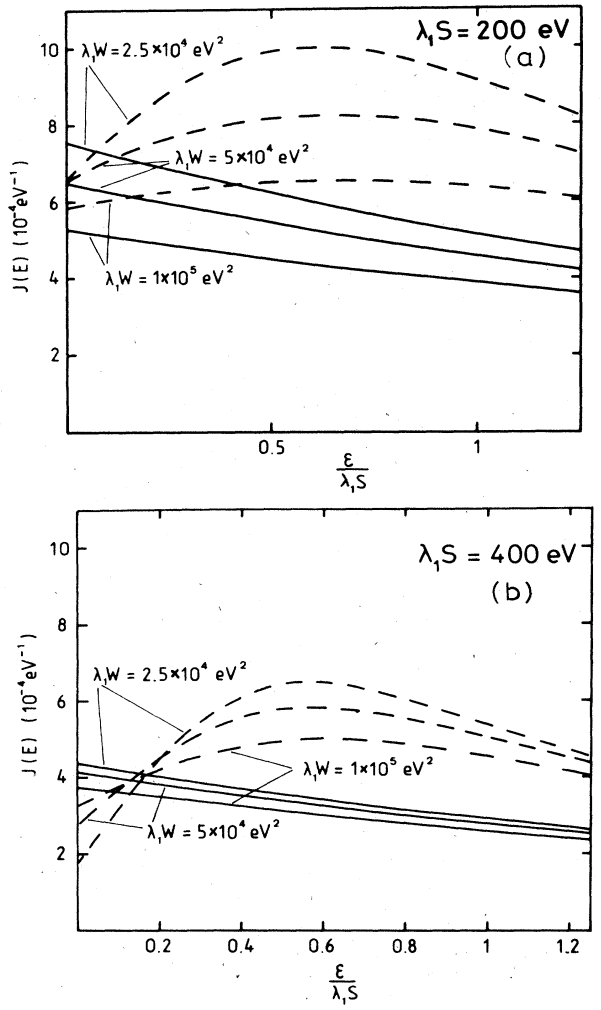

FIG. 7. Continuous energy spectra for several values of $\lambda_1 W$; (a) $\lambda_1 S=200$ eV and (b) $\lambda_1 S=400$ eV. Solid curves: P_1 solution, Eq. (62). Dashed curves: diffusion solution, Eq. (63).

the order of magnitude λ_1 or less. Preliminary investigations show that the diffusion approximation does not agree with measurements,[31] and that the reason essentially is the relatively sharp maximum of the diffusional path-length distribution, cf. Fig. 3, which causes the maximum in the energy distribution, Eq. (63), plotted in Fig. 7.

The P_1 approximation for the path-length distribution deviates strongly from the diffusion solution at relatively small path lengths, as seen in Figs. 3 and 4. However, there exists no definite criterion for when the P_1 approximation is inapplicable, i.e., when it is necessary to proceed to P_L or double P_L approximations of higher order. Nonetheless, it is obvious that the P_1 approximation becomes insufficient at small path lengths corresponding to a few elastic collisions. The path-length distribution for a single, or a few, elastic scattering events can be derived from the Boltzmann equation [Eq. (4)], and a comparison, using atomic elastic scattering cross sections,[28,32] of the P_1 path-length distribution and the distribution for a single elastic collision, shows a good agreement at $R \simeq 0$ for the heavy elements, cf. Fig. 5, where the single-collision distribution with a primary energy of 1000 eV is marked at $R=0$ for platinum and nickel (the lowest value is for nickel). As long as atomic scattering cross sections are applicable for solids, this may show that the P_1 approximation is reasonable for the heavy elements. For the light elements with less elastic scattering, deviations occur at

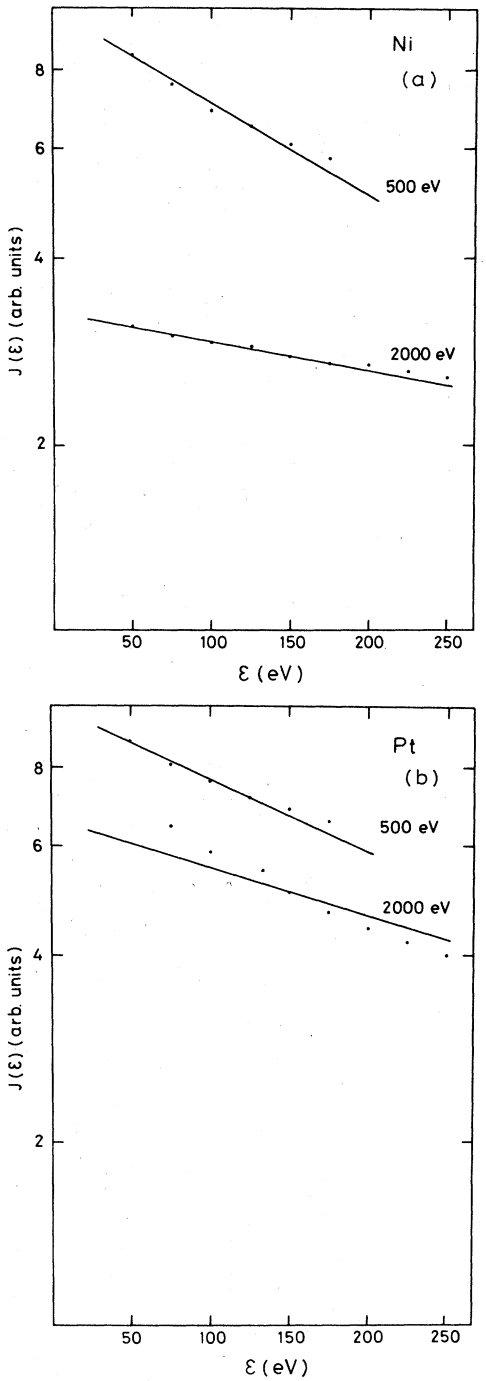

FIG. 8. Continuous energy spectra, straight lines according to Eq. (62), at primary energies of 500 and 2000 eV, respectively, compared with experimental results of Ref. 31. (a) Nickel and (b) platinum.

$R \simeq 0$. Because of the simplicity of the approximate path-length distribution, Eq. (44), it may be applied instead of the full expression, Eq. (41). This leads to the continuous energy distribution, Eq. (62), with a shape, cf. Figs. 7 and 8, similar to that found in EELS measurements[31] (for the continuous part of the spectrum).

Although, a Gaussian energy-loss distribution is possibly not a good description of the energy-loss processes of the electrons, Eqs. (62) and (63) express, however, that small changes in the elastic and inelastic cross sections, due to the dependence upon the decreasing kinetic energy of the moving electrons, have almost no influence on the spectrum because the *ratio* of the cross sections enters. It is noticed that in Eqs. (62) and (63) the parameters λ_1, S, and W enter as S/W, $\lambda_1 S$, and $\lambda_1 W$. This indicates that a variation of the energy distribution is rather moderate toward variations of the parameters from element to element because S and W increase with Z, whereas λ_1 decreases.[25–29]

ACKNOWLEDGMENTS

I would like to thank P. Sigmund and S. Tougaard for valuable suggestions and discussions. Thanks are due M. Urbassek for inspiring suggestions concerning the P_1 approximation and for his interest in the present work. Thanks are also due K. B. Winterbon and L. V. Spencer for useful comments on the manuscript. Financial support from the Ingeborg and Leo Dannin Foundation for Scientific Research is gratefully acknowledged.

APPENDIX A

For a semi-infinite medium, the distribution function at the surface, $x=0$, is given by the uncollided part of the distribution function for positive η. From the transport equation, Eq. (4), with the initial condition (5), it may be deduced that the uncollided part of the distribution function is given by

$$F_u(x,\eta,R)=\delta(x-\eta_0 R)\delta(\eta-\eta_0)e^{-N\sigma R}\,, \tag{A1}$$

where σ is the total elastic scattering cross section. At $x=0$, (A1) reduces to

$$F_u(0,\eta,R)=\delta(\eta_0 R)\delta(\eta-\eta_0)\,, \tag{A2}$$

which explains Eq. (37).

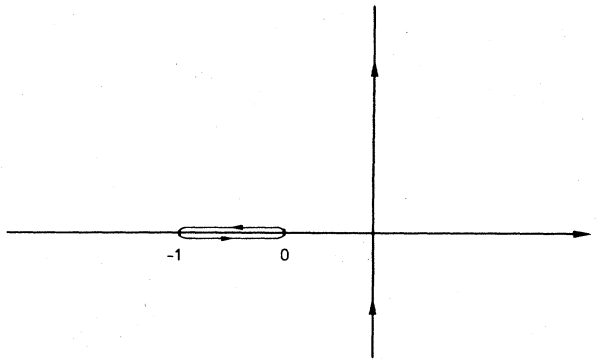

FIG. 9. Integration path in Eq. (B1).

APPENDIX B

Consider Eq. (40), which needs to be Laplace-inverted. The term of interest is

$$\frac{1}{2\pi i}\int_{c-i\infty}^{c+i\infty} ds \frac{e^{sR}}{2/\sqrt{3}+[(s+N\sigma_1)/s]^{1/2}} = \frac{N\sigma_1}{2\pi i}\int_{c-i\infty}^{c+i\infty} du\, e^{uN\sigma_1 R}\frac{2\sqrt{3}u-3\sqrt{u(u+1)}}{u-3}\,, \tag{B1}$$

with $u=s/N\sigma_1$. It is noticed that $u=3$ gives no contribution to the integral and that the only contribution comes from the integration around the branch points -1 and 0, cf. Fig. 9. Thus,

$$\frac{1}{2\pi i}\int_{c-i\infty}^{c+i\infty} ds \frac{e^{sR}}{2/\sqrt{3}+[(s+N\sigma_1)/s]^{1/2}} = -\frac{3N\sigma_1}{\pi}\int_0^1 du\, e^{-uN\sigma_1 R}\frac{\sqrt{u(1-u)}}{u+3}\,. \tag{B2}$$

[1] S. Tougaard and P. Sigmund, Phys. Rev. B **25**, 4452 (1982).
[2] S. Tougaard, Surf. Sci. **139**, 208 (1984); S. Tougaard and B. Jørgensen, *ibid.* **143**, 482 (1984).
[3] H. Froitzheim, in *Electron Spectroscopy for Surface Analysis,* Vol. 4 of *Topics in Current Physics,* edited by H. Ibach (Springer, Berlin, 1977), p. 205.
[4] M. J. Higatsberger, in Advances in Electronics and Electron Physics, edited by C. Marton (Academic, New York, 1981), Vol. 56, p. 291.
[5] J. T. Grant, T. W. Haas, and J. E. Houston, Phys. Lett. **45A**, 309 (1973).
[6] H. E. Bishop, in *Electron Beam Interactions with Solids for Microscopy, Microanalysis, and Microlithography,* edited by D. F. Kyser, H. Niedrig, D. E. Newbury, and R. Shimizu (AMF O'Hare, Chicago, 1984), p. 259.
[7] J. P. Langeron, L. Minel, J. L. Vignes, S. Bouquet, F. Pellerin, G. Lorang, P. Ailloud, and J. le Hériey, Surf. Sci. **138**, 610 (1984).
[8] H. H. Madden and J. E. Houston, J. Appl. Phys. **47**, 3071 (1976).
[9] W. M. Mularie and W. T. Peria, Surf. Sci. **26**, 125 (1971).
[10] E. N. Sickafus, Surf. Sci. **100**, 529 (1980).
[11] R. Hesse, U. Littmark, and P. Staib, Appl. Phys. **11**, 233 (1976).
[12] P. Staib and J. Kirschner, Appl. Phys. **3**, 421 (1974).
[13] R. Shimizu, Y. Kataoka, T. Ikuta, T. Koshikawa, and H. Hashimoto, J. Phys. D **9**, 101 (1976); R. Shimizu, Jpn. J. Appl. Phys. **22**, 1631 (1983).
[14] R. Shimizu and S. Ichimura, Surf. Sci. **133**, 250 (1983).
[15] S. Valkealahti and R. M. Nieminen, Appl. Phys. A **32**, 95 (1983); A **35**, 51 (1984); A. Jablonski, Surf. Sci. **151**, 166 (1985).
[16] P. Sigmund and S. Tougaard, in *Inelastic Particle-Surface Collisions,* Vol. 17 of *Springer Series in Chemical Physics,* edited

by E. Taglauer and W. Heiland (Springer, Berlin, 1981), p. 2.
[17]K. M. Case and P. F. Zweifel, *Linear Transport Theory* (Addison-Wesley, Reading, Mass., 1967).
[18]J. J. Duderstadt and W. R. Martin, Transport Theory (Wiley, New York, 1979).
[19]J. W. Weymouth, Phys. Rev. **84**, 766 (1951).
[20]K. B. Winterbon, P. Sigmund, and J. B. Sanders, Mat.-Fys. Medd. K. Dan. Vidensk Selsk. **37**, No. 14 (1970).
[21]R. E. Marshak, Phys. Rev. **71**, 443 (1947); J. A. Davies, Nucl. Sci. Eng. **27**, 542 (1967).
[22]*Handbook of Mathematical Functions,* edited by M. Abramowitz and I. Stegun (Dover, New York, 1972).
[23]I. Kuščer and P. F. Zweifel, J. Math. Phys. (N.Y.) **6**, 1125 (1965).
[24]L. Landau, J. Phys. (Moscow) **8**, 201 (1944).
[25]J. C. Ashley, C. J. Tung, and R. H. Ritchie, Surf. Sci. **81**, 409 (1979); C. J. Tung, J. C. Ashley, and R. H. Ritchie, *ibid.* **81**, 427 (1979).
[26]A. F. Akkermann and G. Ya. Chernov, Phys. Status Solidi B **89**, 329 (1978).
[27]D. Liljequist, J. Phys. D **16**, 1567 (1983).
[28]M. E. Riley, C. J. MacCallum, and F. Biggs, At. Data Nucl. Data Tables **15**, 443 (1975); **28**, 379 (1983).
[29]N. Bohr, Mat. Fys. Medd. Dan. Vidensk. Selsk. **18**, No. 8 (1948).
[30]C. Møller, Ann. Phys. (Leipzig) **14**, 531 (1932); N. F. Mott, Proc. R. Soc. London Ser. A **126**, 259 (1930).
[31]S. Tougaard (unpublished).
[32]M. Fink and A. C. Yates, At. Data **1**, 385 (1970); M. Fink and J. Ingram, *ibid.* **4**, 129 (1972); D. Gregory and M. Fink At. Data Nucl. Data Tables **14**, 39 (1974).